IMPROVING THE ESTIMATION OF CRS PARAMETERS USING LOCAL SLOPES

L.T. Santos and J. Schleicher

email: *lucio@ime.unicamp.br*

keywords: *Local slopes, CRS, parameter estimation*

ABSTRACT

The complete set of CRS parameters can be extracted from seismic data by an application of modern local-slope-extraction techniques. The necessary information about the CRS parameters is contained in the slopes of the common-midpoint section at the central point and one or several common-offset sections in its vicinity. Here, we improve the extraction technique, eliminating the need for slope derivatives. As demonstrated by a synthetic data example, the slope extraction is sufficiently robust to allow for high-quality extraction of all CRS parameters from the extracted slope fields. In this way, the CRS parameter extraction can be sped up by several orders of magnitude.

INTRODUCTION

Present-day techniques to estimate the traveltime parameters of the common-reflection-surface (CRS) stack rely on local coherence analyses that are tedious and time-consuming processes (see, e.g., Jäger et al., 2001; Hertweck et al., 2007). However, as demonstrated last year (Santos et al., 2008), there is a way to speed up the CRS parameter extraction by several orders of magnitude using local traveltime slopes.

The extraction of traveltime attributes, particularly local slopes, has received strong attention in the recent past, because local slopes directly extracted from prestack data are useful in a variety of seismic imaging processes. Perhaps, the most visible ones are those connected with seismic tomography, in which not only traveltimes but also slownesses of events and possible other time-domain attributes are used to build a velocity model. Most prominent examples are slope tomography (Sword, 1987; Biondi, 1990), stereotomography (Billette and Lambaré, 1998; Billette et al., 2003) and normal-incidence-point (NIP) wave tomography (Duveneck, 2004).

The conventional procedure to extract this slope parameter relies on local slant stacks (Ottolini, 1983a). In this method, a local coherence analysis is carried out at each point in the seismic section along short straight-line elements in all possible directions. The direction with the highest coherence defines the slope value at that point.

However, the local-slant-stack approach to local-slope extraction has a number of drawbacks. First of all, the method has a high computational cost. Since the space of local slopes must be closely sampled, there is a high number of coherence analyses to be carried out. The second drawback lies in the method's sensitivity to the aperture of the local slant stacks. An adequate aperture is problem dependent and thus hard to know in advance. Finally, as demonstrated by Schleicher et al. (2009), the extracted slopes are not always reliable, but can be biased towards too high dips.

Recently, Fomel (2002) presented fast techniques how to extract local slopes and even curvature related traveltime parameters. His technique was later improved by Fomel (2007a,b). Schleicher et al. (2009) compared a set of alternative, faster and more reliable ways to extract local slopes. They showed that local slopes can be extracted faster and more reliably than using local slopes using modern extraction techniques.

Santos et al. (2008) showed how the CRS parameters relate to local slopes in order to speed up their extraction. Of course, this relationship is most straightforward for the emergence angle of the normal ray,

β, since this parameter is nothing else but a local slope. Santos et al. (2008) demonstrated that the slope extraction techniques can be extended to allow for the extraction of the remaining CRS parameters. They how the complete set of CRS parameters can be estimated by the application of modern, more advanced local-slope-extraction techniques, that are several orders of magnitude faster than conventional local coherence analysis.

However, the approach of Santos et al. (2008) relied on the derivatives of the extracted local slopes. Such derivatives can be unstable, leading to errors in the extracted parameter values. In this work, we reformulate their technique and show that the use of slope derivatives can be avoided. Our numerical examples demonstrate that this new procedure improves the values of the extracted parameters.

CRS TRAVELTIMES AND LOCAL SLOPES

The common reflection surface (CRS) stack, first presented in two talks at the 1998 EAGE conference by Hubral et al. (1998a) and by Müller (1998), is based on the same ideas and principles as the conventional common-midpoint (CMP) stack. The basic difference is that a CRS stack uses far more traces than those present in a CMP gather. For each stacking trace location (the central point), the CRS method considers a supergather of source-receiver pairs, arbitrarily located with respect to the central point. In other words, the CRS stack uses not only the CMP gather at the central point, but also neighbouring gathers. In this way, the CMP stacking line turns into a CRS stacking surface.

Of course, in order to make use of the additional data dimension in the off-CMP (or relative midpoint coordinate) direction, we need additional traveltime parameters to describe the stacking surface. In 2D, the general traveltime function in the midpoint-offset domain depends now on three independent parameters. In addition to the normal-moveout (NMO) velocity, there is a parameter related to the local slope of the traveltime curve at zero-offset and one that depends on the reflector curvature. In the CRS stack, these three parameters are determined for each central point and all ZO traveltime samples. The procedure is performed automatically, with no a priori selection of traveltime samples.

In previous works, the three CRS traveltime parameters have been related to physical paramters in the model space (Jäger et al., 2001) or in the data space (Hertweck et al., 2007). In this work, we use the simple mathematical parametrization of Santos et al. (2008). In this parametrization, the (generalized) hyperbolic moveout, i.e., the CRS stacking surface, reads

$$T_{CRS}(x,h) = \sqrt{[T_0 + A\,(x-x_0)]^2 + B\,(x-x_0)^2 + C\,h^2}, \qquad (1)$$

where x and h denote the midpoint and half-offset coordinates of the source and receiver pair, x_0 is the midpoint coordinate of the central point, and $T_0 = T_{CRS}(x_0, 0)$ is the ZO traveltime at the central point. As shown in Hubral et al. (1998b), the parameters A, B and C are related to physical model-space quantities β, K_N and K_{NIP}, referred to as the CRS parameters or attributes, by the relationships

$$A = \frac{2\sin\beta}{v_0}, \quad B = \frac{2T_0\cos^2\beta}{v_0}K_N, \quad \text{and} \quad C = \frac{2T_0\cos^2\beta}{v_0}K_{NIP}, \qquad (2)$$

where v_0 denotes the near-surface medium velocity at the central point. The physical meaning of these parameters are: Angle β is the emergence angle of the ZO ray with respect to the surface normal, and K_N and K_{NIP} are the curvatures of the N- and NIP-waves, respectively (see Hubral, 1983). All these quantities are evaluated at the central point. The N- and NIP-waves are fictitious waves that start at the reflection point of the ZO ray, which is called normal-incident-point or NIP, and propagate upwards along the ZO ray with half the medium velocity. The NIP-wave starts with a point source at NIP, i.e., with a curvature radius of zero, while the N-wave starts with a wavefront that possesses the same curvature as the reflector at NIP.

Observe that parameters A, B, and C depend on T_0 and, that the original CRS parameters β, K_N, and K_{NIP} can be calculated once all three parameters A, B, and C, as well as the near-surface velocity v_0, are known. However, for the detection of the parameters A, B, and C, no knowledge of the near-surface velocity v_0 is required.

In terms of the data-space parameters introduced by Hertweck et al. (2007), parameters A, B, and C are expressed as

$$A = 2p, \quad B = \frac{4}{V_{CMO}^2}, \quad \text{and} \quad C = \frac{4}{V_{NMO}^2} \qquad (3)$$

where p is the local slope at point (x_0, t_0) in the zero-offset section, V_{NMO} is the stacking or NMO velocity, and V_{CMO} is a velocity parameter Hertweck et al. (2007) have termed the curvature move-out (CMO) velocity. The reason for this name is the fact that the corresponding term in equation (1) is zero for a straight reflection event in the zero-offset section.

As shown by Santos et al. (2008), the CRS parameters can be expressed entirely as a function of local slopes of the reflection traveltime surfaces in the CMP section and local slopes and their derivatives in the CO sections. Below, we briefly review their analysis to demonstrate that the derivatives of the local slopes in the CO sections are not needed.

In the following discussion, we will use capital letters T when talking about theoretical traveltime functions and lowercase letters t when talking about time coordinates in seismic sections. Correspondingly, we use lowercase letters, a, b, and c for the CRS parameters when referring to preliminary estimates and reserve the uppercase letters only for the final estimate maps already associated with the central point x_0 and zero-offset traveltime t_0.

Common-midpoint traveltime

The extraction of C from the CMP gather at the central point remains the same as described in Santos et al. (2008). For source-receiver pairs in the CMP gather at $x = x_0$, formula (1) reduces to the weel-known *Normal Moveout (NMO)* function,

$$T_{CMP}(h) = T_{CRS}(x_0, h) = \sqrt{T_0^2 + C\,h^2}. \tag{4}$$

The derivative of equation (4) with respect to source-receiver offset $2h$ yields

$$p = \frac{1}{2}\frac{d}{dh}T_{CMP} = \frac{C\,h}{2\,T_{CMP}}. \tag{5}$$

Thus, if we know the local slope $p = p(h, t)$ at a point (h, t) in a CMP gather, we can use equations (4) and (5) to eliminate C from the moveout equation. This provides us with the NMO coordinate map

$$t_0 = \sqrt{t^2 - 2\,h\,t\,p(h, t)}. \tag{6}$$

which describes the relationship between the coordinates t, h in a CMP section and the corresponding zero-offset time t_0 at x_0. Equation (6) can be immediately used for an automatic NMO correction (Ottolini, 1983b; Schleicher et al., 2009), since it tells us how to move a pixel of information from coordinates (h, t) in the CMP section to (h, t_0) in the NMO corrected section.

On the other hand, equation (5) provides us with the first relationship between a curvature parameter and a local slope. Rewriting equation (5), we see that an estimate of parameter C at half-offset h and time t is given by

$$c(h, t) = \frac{2\,t\,p(h, t)}{h}. \tag{7}$$

From equation (7), we infer the procedure that achieves the determination of parameter C. All that needs to be done is to correct the extracted local slope p at a position (h, t) in the CMP section with the factor $2t/h$ and then to transfer the obtained value of c to the C-parameter section at (x_0, t_0). This can be done fully automatically. Since there is redundant information from all half-offsets, the final $C(x_0, t_0)$ can be calculated by averaging over all $c(h, t)$ that correspond to the same (x_0, t_0). In our numerical examples, this averaging uses the semblance of p at (h, t) as a weight function.

Common-offset traveltime

The extraction of parameters A and B from a common offset (CO) gather with fixed $h_0 \neq 0$ in the vicinity of the central point can be improved over the procedure described in Santos et al. (2008). For the case of a CO gather with a fixed half-offset $h = h_0 \neq 0$, formula (1) reduces to

$$T_{CO}(x) = T_{CRS}(x, h_0) = \sqrt{T_{CMP}(h_0)^2 + 2\,A\,T_0\,(x - x_0) + D\,(x - x_0)^2}, \tag{8}$$

where the new parameter D is given by

$$D = A^2 + B, \tag{9}$$

and T_{CMP} is the traveltime for the offset ray with midpoint at x_0. It is given in terms of the ZO traveltime t_0 by equation (4) with $h = h_0$.

From traveltime formula (8), we see that the local slope q at a point (x, t) in the CO gather is given by

$$q = \frac{d}{dx} T_{CO} = \frac{A\, T_0 + D\, (x - x_0)}{T_{CO}}. \tag{10}$$

Instead of following the path of Santos et al. (2008) and taking the derivative of equation (10) to isolate D, we recognize that at $x = x_0$, this equation reduces to

$$AT_0 = q(x_0, t)\, t, \tag{11}$$

which, in turn, can be used to rewrite equation (10) as

$$D(x - x_0) = t\, [q(x, t) - q(x_0, t)]. \tag{12}$$

Therefore, substituting the above expressions in equation (8) and solving for the CMP traveltime, we obtain the coordinate map

$$t_{CMP} = \sqrt{t^2 - t\, (x - x_0)\, [q(x, t) + q(x_0, t)]}, \tag{13}$$

between the CO and CMP sections. Map (13) can be executed once q has been detected at every point (x, t) in the CO section. As a last step, the time coordinate t_{CMP} must be related to its associated ZO traveltime t_0. This can be done using formula (6), i.e.,

$$t_0 = \sqrt{t_{CMP}^2 - 2\, h_0\, t_{CMP}\, p(h_0, t_{CMP})}, \tag{14}$$

where $p(h_0, t_{CMP})$ is the local slope at the coordinates $h = h_0$ and $t = t_{CMP}$ in the CMP section at x_0, extracted in the preceeding step.

Combining the above equations and coordinate maps, formulas (9), (11) and (12), we can determine estimates $a(x, t)$ and $b(x, t)$ for each point (x, t) in the CO section according to

$$a(x, t) = \frac{t\, q(x_0, t)}{t_0}, \tag{15}$$

and

$$b(x, t) = \frac{t\, [q(x, t) - q(x_0, t)]}{x - x_0} - a(x, t).^2, \quad x \neq x_0, \tag{16}$$

Note that all these estimates $a(x, t)$ and $b(x, t)$ pertain to the one chosen central point x_0. Therefore, they still need to be transfered to the point (x_0, t_0) in the parameter sections. As before for the case of the C section, many estimates of $a(x, t)$ and $b(x, t)$ will be attributed to the same ZO time t_0. Thus, $A(x_0, t_0)$ and $B(x_0, t_0)$ need to be calculated by averaging over all $a(h, t)$ and $b(x, t)$, respectively, that correspond to the same (x_0, t_0). Again, our numerical implementation of this averaging uses semblance weights.

For the extraction of A and B, further data redundancy is avaliable. The mapping procedure described here for a single constant half-offset h_0 can be applied for different CO sections around the central point x_0. The final values of A and B can then be obtained by averaging over all values that are attributed to the same point (x_0, t_0) from all different CO sections used in the process.

Extracting the local slopes

The extraction of local slopes is done by so-called plane-wave destructors. The differential equation that describes a local plane-wave event in a seismic section is given by (Claerbout, 2004)

$$\psi_y(y, t) + s\, \psi_t(y, t) = 0, \tag{17}$$

where $\psi(y, t)$ is the wavefield, t is the time coordinate, and y is the horizontal coordinate, i.e., offset $(2h)$ in the case of a CMP section or midpoint (x) in the case of a CO section. Quantity s represents the local slope (i.e., p or q in a CMP or CO section), which may depend on y and even on t, i.e., generally, $s = s(y, t)$. To extract the slopes, we use the technique presented in Schleicher et al. (2009) with the modification reported in Santos et al. (2008).
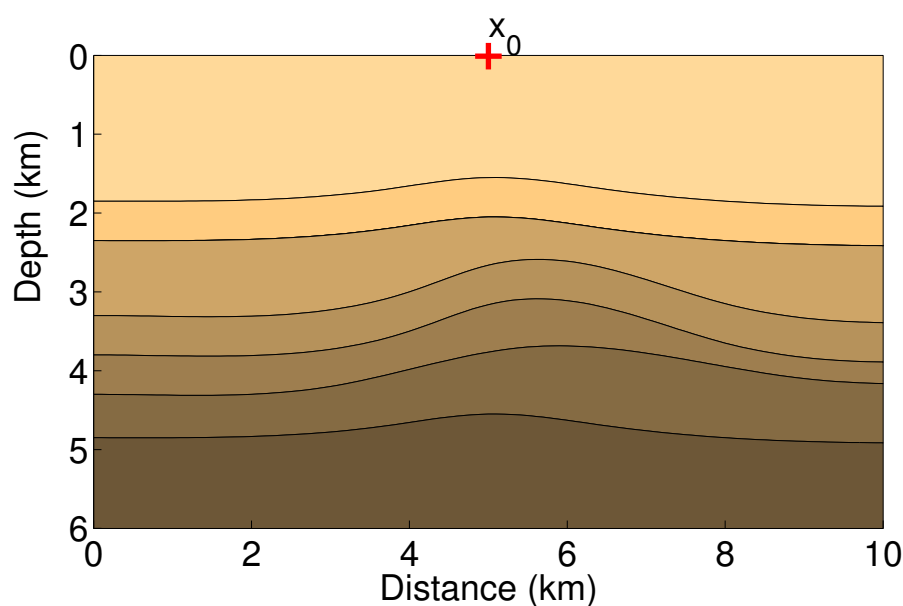
Figure 1: Synthetic model for the experiments.

SYNTHETIC EXAMPLES

For the numerical experiments we used the same simple synthetic model as in Santos et al. (2008). It consists of a stratified medium with five homogeneous layers between two homogeneous half-spaces (see Figure 1). We simulated CMP sections with 100 half-offsets ranging from -1 km to 1 km, and CO sections with half-offsets ranging from 100 m to 500 m, each containing 51 midpoints around the respective central point. In all simulations the time sampling was 4 ms. For better control over the CRS parameters, we simulated all reflection events as if the velocities in the model where constant rms velocities down to the corresponding reflector. The rms velocity for the shallowest reflector was 4.0 km/s, increasing by 0.2 km/s for each layer to 5.0 km/s for the deepest one. For the noisy examples, we added random white noise with a signal-to-noise ratio of 3 to the sections.

Analysis at a single central point

We start by comparing the results of the improved extraction technique described above (below referred to as the "new technique") to those obtained with the previous one of Santos et al. (2008) (below called the "old technique") at a single central point $x_0 = 5$ km. This central point is also shown in Figure 1.

The results of the CRS parameter extraction for noise-free data, using old and new techniques are shown in Figure 2. The extracted values (red lines) are depicted together with the respective exact values (blue crosses). Of course, true values are only available at the reflection events while the extraction procedure yields values at all times. This figure also shows the values of the accumulated semblances (S) for p and q. These are the mean values of the semblances of all values of the parameters A, B and C that contributed to the final values. As usual for noise-free data, the semblance is very high everywhere. Comparing the figure parts, we see that the extraction of C and A with both procedures yielded equivalent results, while the values of B extracted using the new technique are significantly better.

The corresponding results using noisy data are shown in Figure 3. As we can see in these figures, the presence of noise does not alter the above observations. The results are still highly satisfactory. Parameters A and C have lost almost no quality in comparison to the noise-free situation (Figure 2). In both techniques, the noise seems to influence mainly the extracted values of parameter B. However, its deterioration is much stronger when extracted with the old technique.

It is to be noted that for the noisy data, the accumulated semblance S exhibits significant peaks at the actual reflection times, thus carrying useful information on where the extracted parameter values are
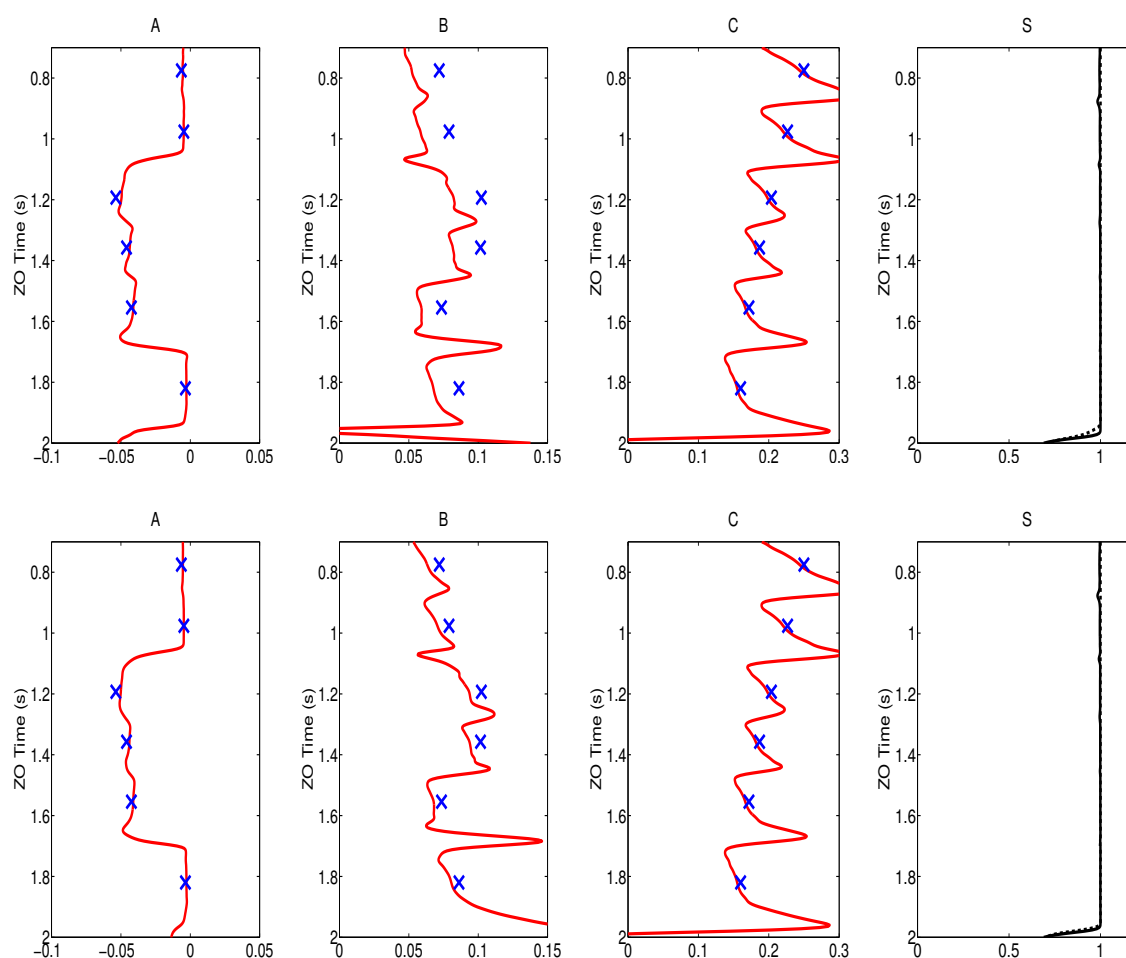
Figure 2: Experiments without noise: CRS parameters (A, B, C) and semblances (S). The exact are the blue crosses and the estimated ones are the red lines. Top: old technique; bottom: new technique.

actually reliable. This behaviour is the same for both techniques.

These numerical experiments demonstrate that the estimation of CRS parameters from local slopes is sufficiently stable to permit their automatic extraction, even for noisy data. The new technique allows to extract C and A of the same quality as before while significantly improving B. The new technique is even a little faster than the old one because it doesn't need to calculate slope derivatives. We stress again that this extraction procedure is orders of magnitude faster than the conventional CRS method that uses local coherence analyses.

Since the noise deteriorates the quality of the extracted CRS parameters, we also tested the idea of stabilizing the extraction by using a number of common-offsets. The results using five common-offset sections with half-offsets from 100 m to 500 m are shown in Figure 4. As expected, the use of more information stabilizes the parameter extraction for both the old and the new procedure. The new technique still improve the quality of the extracted values for parameter B.

Parameter Sections

To demonstrate the quality of the proposed parameter extraction, we repeated the above experiments for 141 central points between 1 km and 7 km along the model of Figure 1. Figure 5 shows the parameter panels resulting from the new extraction technique applied to the noise-free data. The panels as masked with the semblance section, muting all parameter values at points where the semblance value is below 0.9.
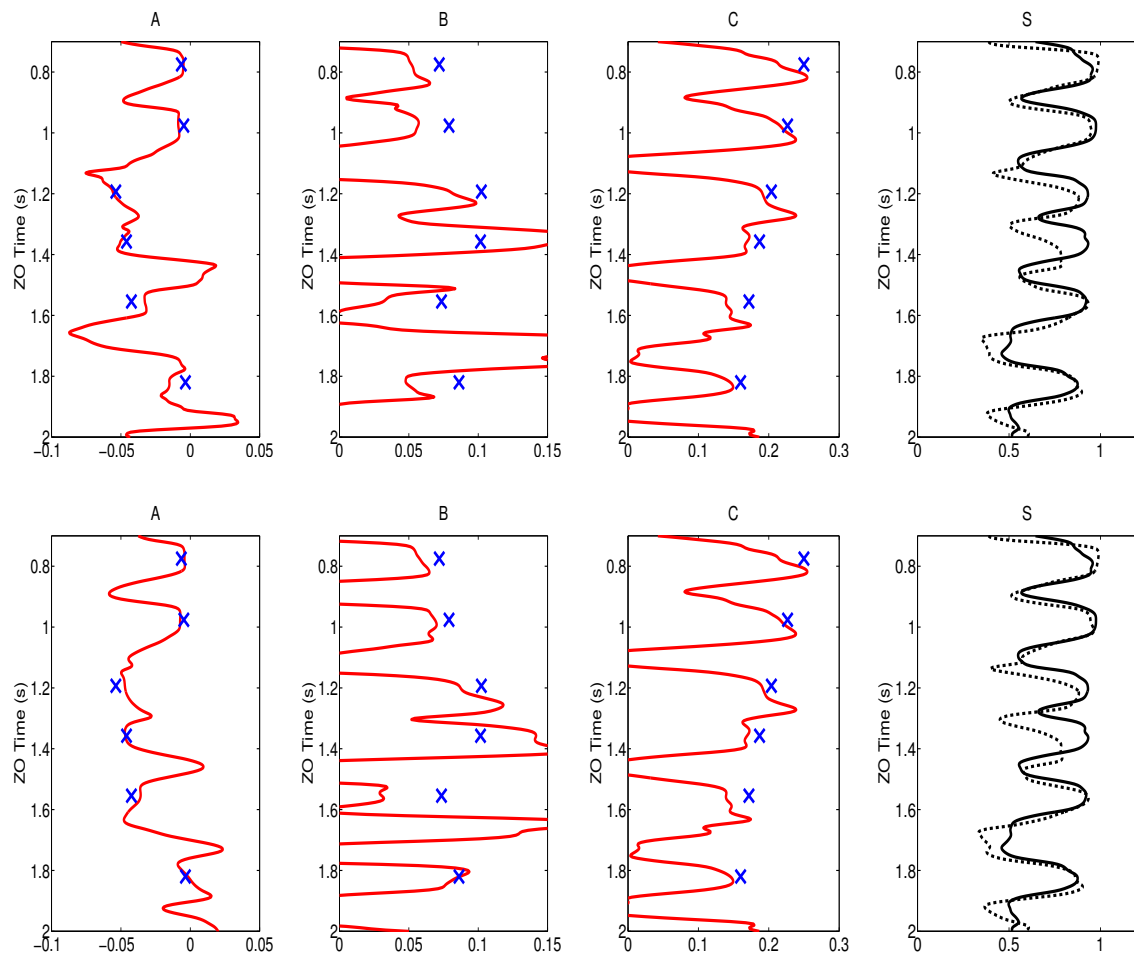
Figure 3: Experiments with 30% added noise: CRS parameters (A, B, C) and semblances (S). The exact are the blue crosses and the estimated ones are the red lines. One Offset. Top: old technique; bottom: new technique.

Also shown in Figure 5 are the posions of the reflection events in the zero-offset section (black lines). All three parameter panels exhibit the expected behaviour. The A section contain negative (blue) values where the events dip to the left and positive (red) values where the events dip to the right. The B section exhibits the corresponding behaviour for positive and negative curvatures. Finally, the C section exhibits decreasing values from top to bottom, in correspondence with the increasing rms velocity in the model.

Figure 6 demonstrates that the quality of the parameter extraction remains almost unaltered for a noise level of 30% (SNR = 3). The depicted panels where obtained using five CO sections. The basis features and even the extracted values of the parameters remain the same. The semblance level for the masking was reduced for these figures to 0.7.

For a more quantitative analysis of the extracted parameter values, we plot in Figure 7 the values of A and B along the reflection event of the deepest reflector. Shown as black solid lines are the exact values. We see in the top row (noise free data) that the new technique (red solid lines) yields practically the same values of A, and improved values of B when compared to the old technique (blue dashed lines). For the noisy data (bottom row) A is again of the same quality in both techniques. Concerning B, we notice that the new technique not only improves the values but also reduces the fluctuations.
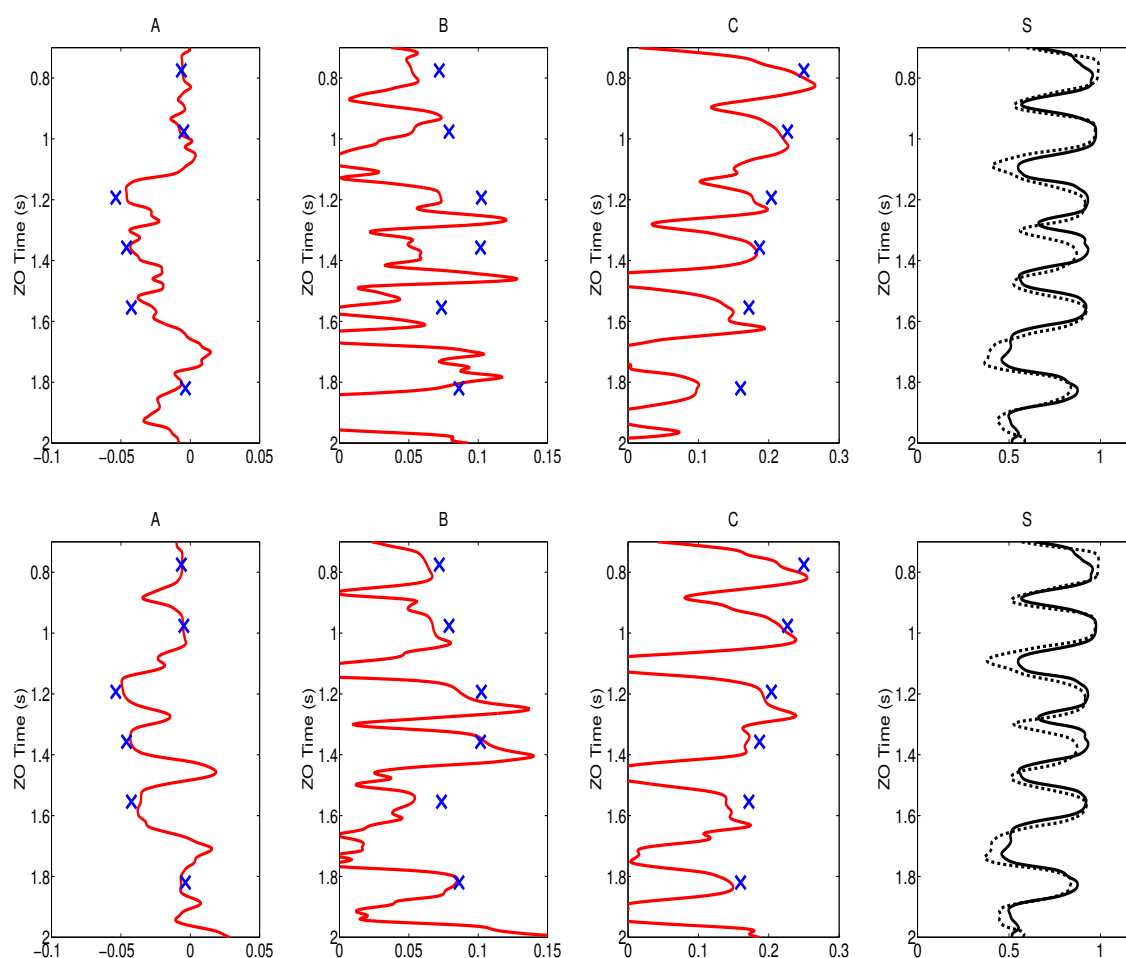
Figure 4: Experiment with five offsets with 30% added noise: CRS parameters (A, B, C) and semblances (S). The exact are the blue crosses and the estimated ones are the red lines. Top: old technique; bottom: new technique.

CONCLUSIONS

CRS parameter extraction by local coherence analysis has a number of drawbacks. First and most important of all, the method has a high computational cost. Since the space of possible parameter values must be closely sampled, there is a high number of coherence analyses to be carried out. The second drawback lies in the method's sensitivity to the aperture of the local stacking operators. An adequate aperture is problem dependent and thus hard to know in advance.

In a previous work, we showed that it is possible to overcome these problems by a different approach to parameter extraction. Here, we have improved the extraction technique. We have presented an application of modern local-slope-extraction techniques so as to allow for the detection of the complete set of CRS parameters. The necessary information about the CRS parameters is contained in the slopes of the common-midpoint and common-offset sections at the central point. As demonstrated by a synthetic data example, the slope extraction is sufficiently robust to allow for high-quality extraction of all CRS parameters from the extracted slope fields. In this way, the CRS parameter extraction can be sped up by several orders of magnitude.
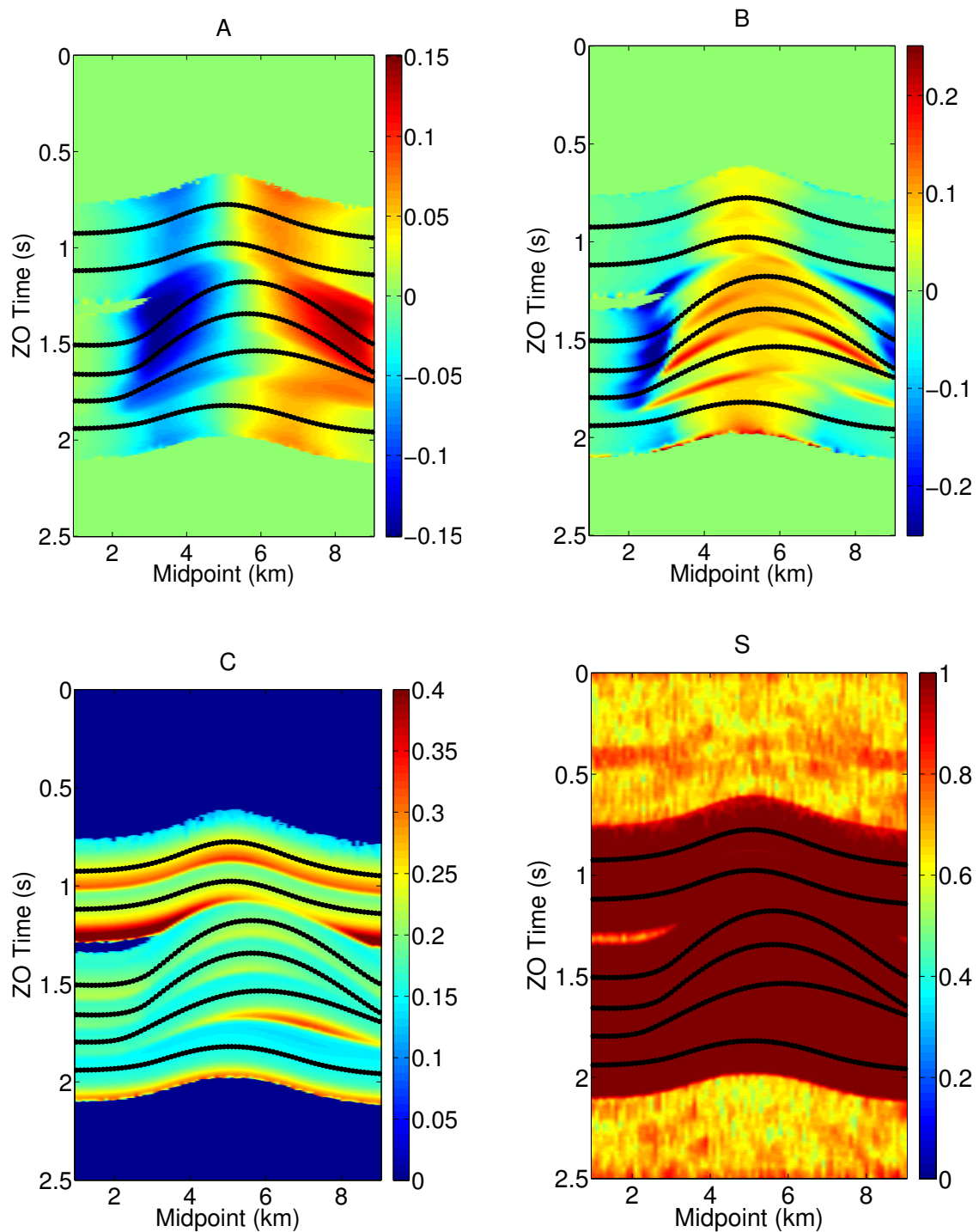
Figure 5: CRS parameters and semblance sections for data without noise. Parameter values at points where semblance is below 0.9 were muted.
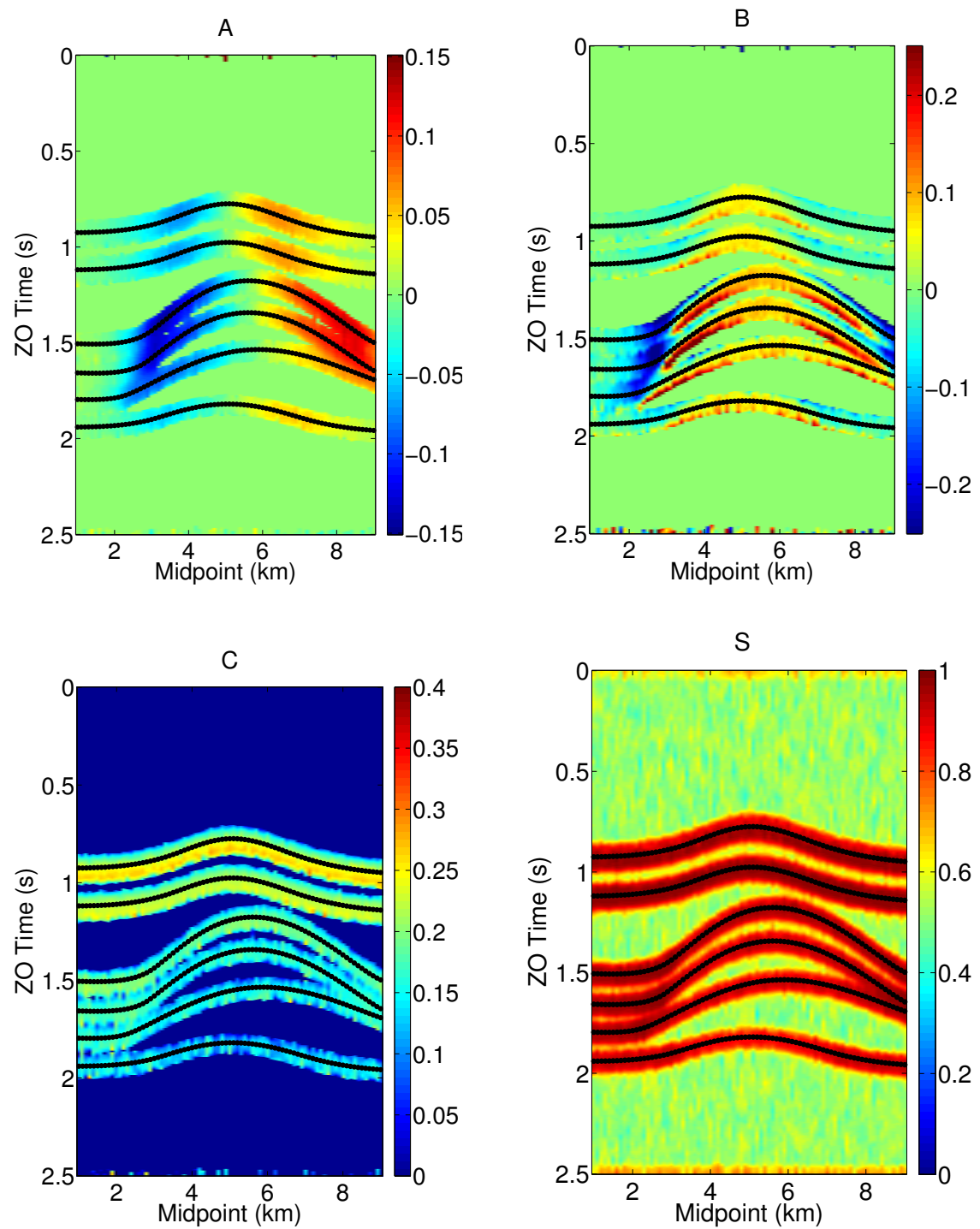
Figure 6: CRS parameters and semblance sections for data with 30% noise. Parameter values at points where semblance is below 0.7 were muted.
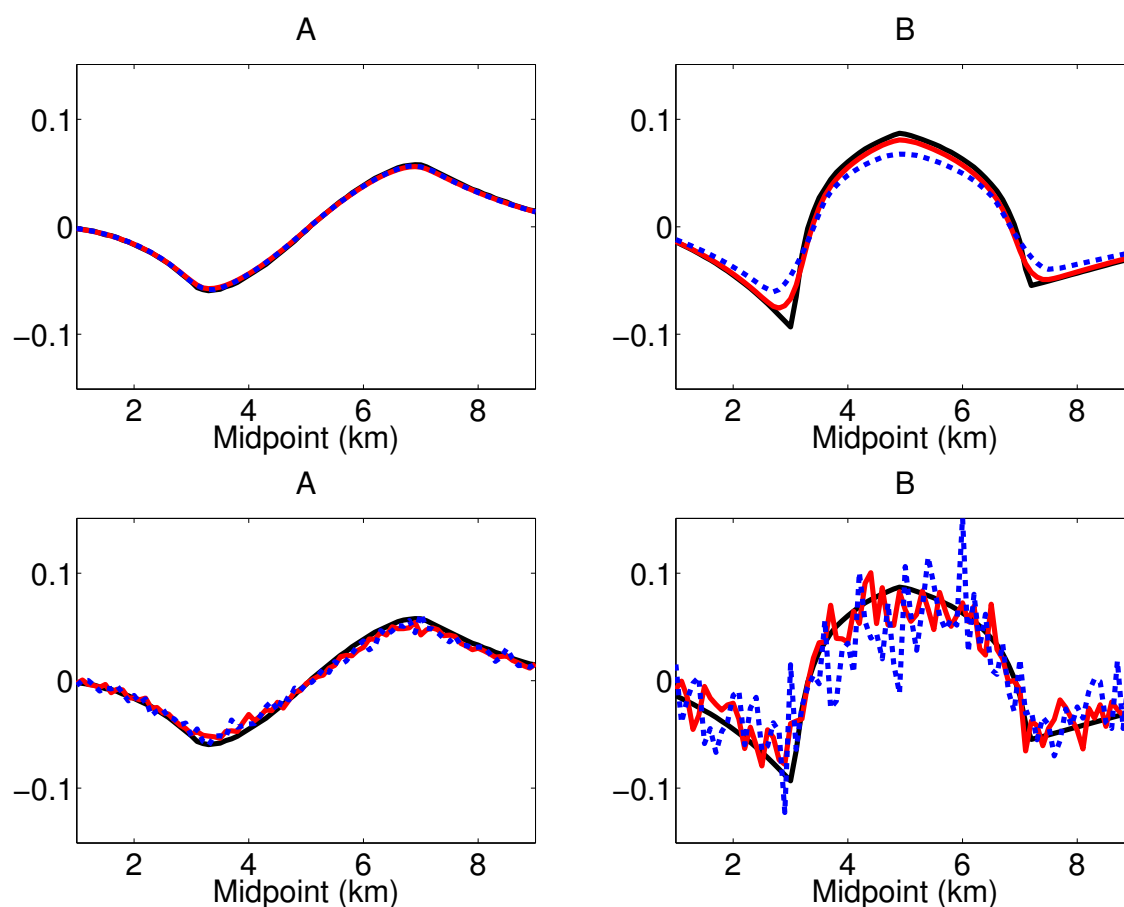
Figure 7: Parameters A and B along the ZO reflection event for the deepest reflector. Top: no noise; bottom: 30% noise.

ACKNOWLEDGMENTS

REFERENCES

Billette, F. and Lambaré, G. (1998). Velocity macro-model estimation from seismic reflection data by stereotomography. *Geophys. J. Int.*, 135(2):671–690.

Billette, F., Le Bégat, S., Podvin, P., and Lambaré, G. (2003). Practical aspects and applications of 2D stereotomography. *Geophysics*, 68(3):1008–1021.

Biondi, B. (1990). *Seismic velocity estimation by beam stack*. PhD thesis, Stanford University.

Claerbout, J. F. (2004). *Earth Sounding Analysis: Processing versus Inversion*. Blackwell Scientific Publications.

Duveneck, E. (2004). 3D tomographic velocity model estimation with kinematic wavefield attributes. *Geophysical Prospecting*, 52:535–545.

Fomel, S. (2002). Applications of plane-wave destruction filters. *Geophysics*, 67:1946–1960.

Fomel, S. (2007a). Shaping regularization in geophysical-estimation problems. *Geophysics*, 72:R29–R36.

Fomel, S. (2007b). Velocity-independent time-domain seismic imaging using local event slopes. *Geophysics*, 72:S139–S147.

Hertweck, T., Schleicher, J., and Mann, J. (2007). Data stacking beyond CMP. *The Leading Edge*, 26(7):818–827.

Hubral, P. (1983). Computing true amplitude reflections in a laterally inhomogeneous earth. *Geophysics*, 48:1051–1062.

Hubral, P., Höcht, G., and Jäger, R. (1998a). An introduction to the common reflection surface stack. In *60th Conference & Exhibition, Europ. Assoc. Geosci. Eng.* Session 1-19.

Hubral, P., Höcht, G., and Jäger, R. (1998b). An introduction to the common reflection surface stack. *60th EAGE Conference & Exhibition, Expanded Abstracts*, Session:01–19.

Jäger, R., Mann, J., Höcht, G., and Hubral, P. (2001). Common-reflection-surface stack: Image and attributes. *Geophysics*, 66(1):97–109.

Müller, T. (1998). Common Reflection Surface Stack versus NMO/Stack and NMO/DMO/Stack. In *60th Conference & Exhibition, Europ. Assoc. Geosci. Eng.* Session 1-20.

Ottolini, R. (1983a). Signal/noise separation in dip space. *SEP report*, SEP-37:143–149.

Ottolini, R. (1983b). Velocity independent seismic imaging. *SEP report*, SEP-37:59–67.

Santos, L. T., Schleicher, J., Costa, J. C., and Novais, A. (2008). Fast estimation of CRS parameters using local slopes. *Annual WIT Report*, 12:219–229.

Schleicher, J., Costa, J. C., Santos, L. T., Novais, A., and Tygel, M. (2009). On the estimation of local slopes. *Geophysics*, 74:P25–P33.

Sword, C. H. (1987). *Tomographic determination of interval velocities from reflection seismic data: The method of controlled directional reception*. PhD thesis, Stanford University.